

Article

Friction Stir Spot Butt Welding of Dissimilar S45C Steel and 6061-T6 Aluminum Alloy

Kun Gao ¹, Shengwei Zhang ¹, Mounarik Mondal ¹, Soumyabrata Basak ¹, Sung-Tae Hong ^{1,*}
and Heechan Shim ²

¹ School of Mechanical Engineering, University of Ulsan, Ulsan 44610, Korea; 18217603739@163.com (K.G.); zsw19900619@gmail.com (S.Z.); mondal.mounarik3@gmail.com (M.M.); sb34@iitbbs.ac.in (S.B.)

² Materials R&D Center, ILJIN Global Co. R&D Center, Seoul 06157, Korea; shinheechan@iljin.com

* Correspondence: sthong@ulsan.ac.kr; Tel.: +82-052-259-2148

Abstract: Friction stir spot welding (FSSW) of dissimilar S45C steel and 6061-T6 aluminum alloy in a butt configuration is experimentally investigated. Butt spot welding is performed using a convex scrolled shoulder tool at different tool rotational speeds. FSSW butt joints are successfully fabricated by offsetting the tool to the steel side. The microstructures of the joints fabricated at three different tool rotational speeds are characterized using scanning electron microscopy and energy dispersive spectrometry. Microstructural analysis shows the presence of intermetallic compounds (IMCs) along the steel/aluminum interface. The thickness of the IMC layer and the tensile strength of the joint increase with increasing the tool rotational speed. The results of tensile tests and microstructural analysis show that the joint performance is closely related to the IMCs at the joint interface.

Keywords: friction stir spot butt welding; aluminum alloy; steel; dissimilar joint; intermetallic compounds



Citation: Gao, K.; Zhang, S.; Mondal, M.; Basak, S.; Hong, S.-T.; Shim, H. Friction Stir Spot Butt Welding of Dissimilar S45C Steel and 6061-T6 Aluminum Alloy. *Metals* **2021**, *11*, 1252. <https://doi.org/10.3390/met11081252>

Academic Editor: Aleksander Lisiecki

Received: 15 July 2021

Accepted: 5 August 2021

Published: 7 August 2021

Publisher's Note: MDPI stays neutral with regard to jurisdictional claims in published maps and institutional affiliations.



Copyright: © 2021 by the authors. Licensee MDPI, Basel, Switzerland. This article is an open access article distributed under the terms and conditions of the Creative Commons Attribution (CC BY) license (<https://creativecommons.org/licenses/by/4.0/>).

1. Introduction

Incorporation of lightweight materials for manufacturing various automotive components has been increasing to meet regulations of lower emissions and better fuel efficiency, while simultaneously resolving safety issues [1]. Among various lightweight materials, aluminum alloys are widely used for their formability and cost-effectiveness [2]. Although aluminum alloys provide various advantages, they are not able to replace steels completely. In many industrial applications, it is very difficult or nearly impossible for lightweight aluminum alloys alone to fulfill imposed structural or mechanical requirements. As a result, steels, which have superior mechanical properties and cheaper prices than aluminum alloys, still have wide applications in the automobile, aerospace, and railway industries. Therefore, to achieve weight reduction while satisfying the structural or mechanical requirements, the joining of dissimilar steel and aluminum alloys is unavoidable in many industrial applications [3].

However, the joining of these two alloys imposes complications due to the vast differences in their thermomechanical properties and their tendency to form brittle intermetallic compounds (IMCs) [4]. Researchers have attempted to join steels and aluminum alloys using two different joining methods: conventional fusion welding and solid-state joining. Conventional fusion welding methods, such as resistance spot welding [5], tungsten inert gas brazing [6], and laser welding [7], have been utilized to join steels and aluminum alloys. However, technical difficulties, including the formation of complex weld pool structures, inhomogeneous solidification microstructures, and segregation, hinder their practical applications. Moreover, most conventional fusing welding techniques involve relatively high heat input, resulting in the formation of a thick layer of brittle IMCs [4,8,9]. Since fatigue cracks generally originate inside the brittle IMC layer, researchers have recommended limiting the thickness of the IMC layer to less than 10 µm to achieve mechanically sound joints [10–12].

In contrast, solid-state joining methods, such as explosion welding, friction welding, riveted–adhesive hybrid joining technique, and electrically assisted pressure joining, avoid melting of the alloys and thereby avert most solidification defects [13–18]. Nevertheless, due to the need for high pressure to induce large deformation of materials and also to comply with safety restrictions, explosion welding [17] and friction welding [15] are generally limited to welding components made of highly ductile materials with simple shapes. Electrically assisted pressure joining produces joints by establishing diffusion bonding under the joining conditions of plastic deformation and elevated temperature, which is generally necessary to extend the longer diffusion time to enhance the bonding strength [16]. Riveted–adhesive hybrid joining technique includes two joining methods of adhesive and riveting to enhance the reliability of joint, but it undoubtedly increases the process and causes the rise of cost [18].

Friction stir welding (FSW), which is a solid-state joining technology [19], uses a rotating tool that contacts the workpiece and generates frictional heat to plasticize the material. The rotating tool establishes material flow to accomplish the joining [20]. FSW is generally used to produce butt or lap joints along the length of the workpieces [21–25]. However, depending on the geometry of a complex target structure, spot welding (friction stir spot welding (FSSW)) in a butt configuration can be more effectively used since traverse motion of the tool is not required in spot welding.

In FSW or FSSW of aluminum alloy and steel in a butt configuration, due to the drastically different mechanical and thermomechanical properties of the joining materials, the joining process is usually conducted with an offset to the aluminum alloy side or the steel side. In other words, the initial contact point of the pin of the rotation tool is not at the joining line of the butt configuration. Therefore, in addition to conventional process parameters such as tool rotational speed, welding speed, plunge depth, and tilt angle, the tool offset can also profoundly affect the quality of aluminum/steel joints in FSW or FSSW butt joining [21]. Watanabe et al. [22] studied the influence of tool offset on joint strength of SS400 mild steel and 5083 aluminum alloy and obtained the highest joining strength by offsetting the tool by 0.2 mm toward the steel sheet side. In a study by Kimapong and Watanabe [23], increasing the temperature of the steel by offsetting the tool to the steel side increased the atomic diffusion in the aluminum/steel interface to form the IMC layer.

In FSW or FSSW butt joining, the formation of the IMC layer can significantly affect the performance of the joint. Fereiduni et al. [24] reported that the tool rotational speed and dwell time influenced the formation of IMCs during the FSSW of 5083 aluminum and St-12 alloy sheets, and they obtained the maximum tensile strength with the formation of a 2.3 μm thick IMC layer. Coelho et al. [25] studied the joining of 6181-T4 aluminum alloy to DP600 and HC260LA high-strength steels; they found that heat input and high shear strain played a crucial role in the formation of IMCs. Bozzi et al. [26] reported that the critical thickness of the IMC layer at the friction stir spot welded joint interface of 6016 aluminum alloy and interstitial free steel influenced the shear strength of the joint. Pourali et al. [27] studied IMCs in FSW of 1100 aluminum alloy and St-37 steel plates. They concluded that Fe-rich IMCs with a certain thickness, such as FeAl and Fe₃Al, were not detrimental to the shear strength of the joint. Kaushik et al. [28] studied the effect of tool geometry on the IMC layer evolution during FSW of 5052 aluminum alloy and low-carbon steel.

Previous works related to the FSW of aluminum alloy and steel generally reported on linear welding at the butt or lap position and spot welding (FSSW) at the overlapped position. To our knowledge, research works to date have rarely reported on FSSW of aluminum alloy and steel in a butt configuration. Therefore, based on the specific need for the manufacture of bimaterial automotive components, the FSSW of aluminum alloy and steel in a butt configuration is studied here.

2. Experimental Set-Up

Commercially available S45C steel and 6061-T6 aluminum alloy (AA6061-T6) sheets were selected as the subject materials of the present study (chemical compositions in Table 1). These

materials were cut to a cuboid shape with dimensions (in mm) of 100 (length) \times 40 (width) \times 2 (thickness) and were used as base materials (BMs) for the proposed butt FSSW.

Table 1. Chemical compositions and mechanical properties of AA6061-T6 and S45C steel.

Chemical Composition (wt%)											
Materials	C	P	S	Al	Si	Mn	Fe	Mg	Cu	Cr	Zn
S45C	0.04	0.01	0.003	0.02	0.002	0.15	Bal.	-	-	-	-
AA6061-T6	-	-	-	Bal.	0.6	0.11	0.4	0.9	0.23	0.17	0.04
Mechanical properties											
Materials	Yield stress (MPa)			Tensile strength (MPa)			Elongation at fracture (%)				
S45C	343			569			16				
AA6061-T6	276			310			17				

Prior to joining, the BMs were carefully ground with 320-grit sandpaper to remove the oxide layer and thoroughly degreased with ethanol and acetone. A custom-made FSW machine (RM1A; Bond Technologies, Elkhart, IN, USA) was used to perform FSSW using a spark plasma sintered tungsten carbide (WC) tool (tool geometry in Table 2) on the designated materials in a butt configuration, as depicted in Figure 1a,b. As described in [29,30], alterations of the tool rotational speed and the tool offset significantly influence the material flow and formation of IMCs between the steel and aluminum alloy by varying the heat input and straining of materials during joining. Therefore, the FSSW was performed here by varying these two process parameters (in Table 3), while other parameters, including tool plunging rate, depth of penetration, and dwell time, were kept constant.

Table 2. Geometry of the FSW tool.

Tool Geometry	Dimension
Shoulder diameter (mm)	14.3 mm
Pin height (mm)	0.6 mm
Pin diameter (mm)	2.0 mm
Shoulder type	Convex scrolled shoulder

Table 3. Process parameters for FSSW of AA6061-T6 and S45C steel.

No.	Penetration Depth (mm)	Dwell Time (s)	Temperature Condition (°C)	Tool Plunging Rate (mm/min)	Tool Offset	Rotational Speed (rpm)
1						1400
2					-1.5 mm	1550
3						1700
4			Room temperature			1400
5	1.7	3	(~25)	10	0	1550
6						1700
7						1400
8					+1.5 mm	1550
9						1700
10						1850

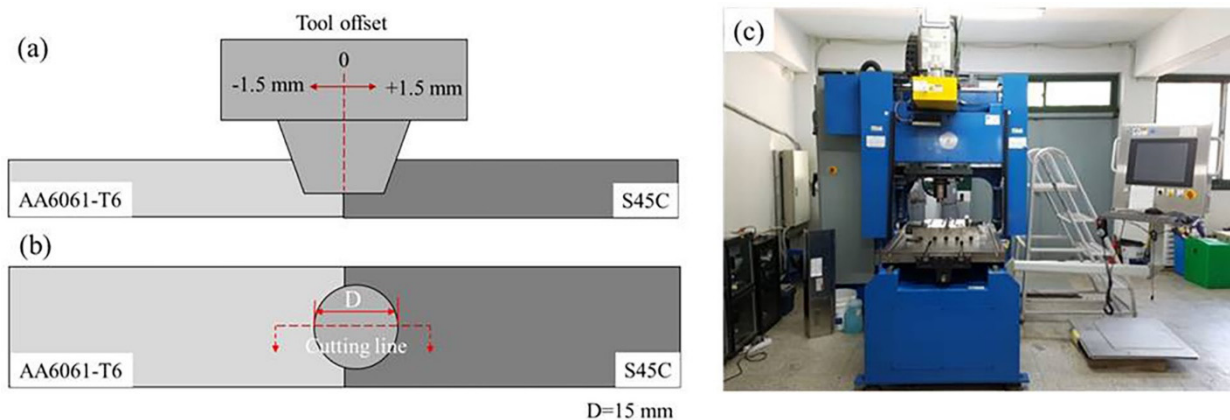


Figure 1. Schematics of specimen configuration: (a) side and (b) top views; (c) FSSW machine.

After FSSW, the quality of the joints was first visually inspected. Subsequently, the weld spots were cut through the joint center (red dotted line in Figure 1b) and were ground and polished for microstructural observation by optical microscopy (OM) (A1M Axio Imager; Carl Zeiss, Göttingen, Germany). The cross-sections of the joints were also examined using a field emission scanning electron microscope (FE-SEM) (SU-70; Hitachi, Tokyo, Japan) equipped with an energy dispersive spectrometer (EDS) (X-Max50; Horiba, Kyoto, Japan).

The friction stir spot welded specimens were commonly notched at both sides, as the welding was performed at the butt position. To avoid the stress concentration by the notch effect during quasistatic tensile testing to evaluate the mechanical properties of the joints, the friction stir spot welded joints were machined to the dimensions of (in mm) 120 (length) \times 10 (width) \times 2 (thickness) before tensile testing, as shown in Figure 2. The tensile strength of each joint was evaluated by using a universal testing machine with a constant displacement rate of 0.5 mm/min. Fracture surfaces of the tensile-tested joint specimens were investigated by SEM and were also detailed with EDS elemental analysis.



Figure 2. Dimensions for a tensile specimen from a butt FSSW joint.

3. Results and Discussion

The appearance (top view) of the friction stir spot welded dissimilar joints of S45C steel and AA6061-T6 with different process parameters is shown in Figure 3. As summarized in Table 4, visual inspection of the joints confirmed that the tool position and tool rotational speed affected the shape and appearance of the weld surfaces.

When the tool was offset by 1.5 mm toward the AA6061-T6 side, evident defects, including surface cracks and partial fusion, were observed, as shown in Figure 3a–c. At relatively low tool rotational speeds (1400 and 1550 rpm), the AA6061-T6 was fused, which suggests that excessive heat was applied to the aluminum alloy during FSSW. Naturally, when increasing the tool rotational speed to 1700 rpm (Figure 3b), partial melting of the AA6061-T6 was aggravated.

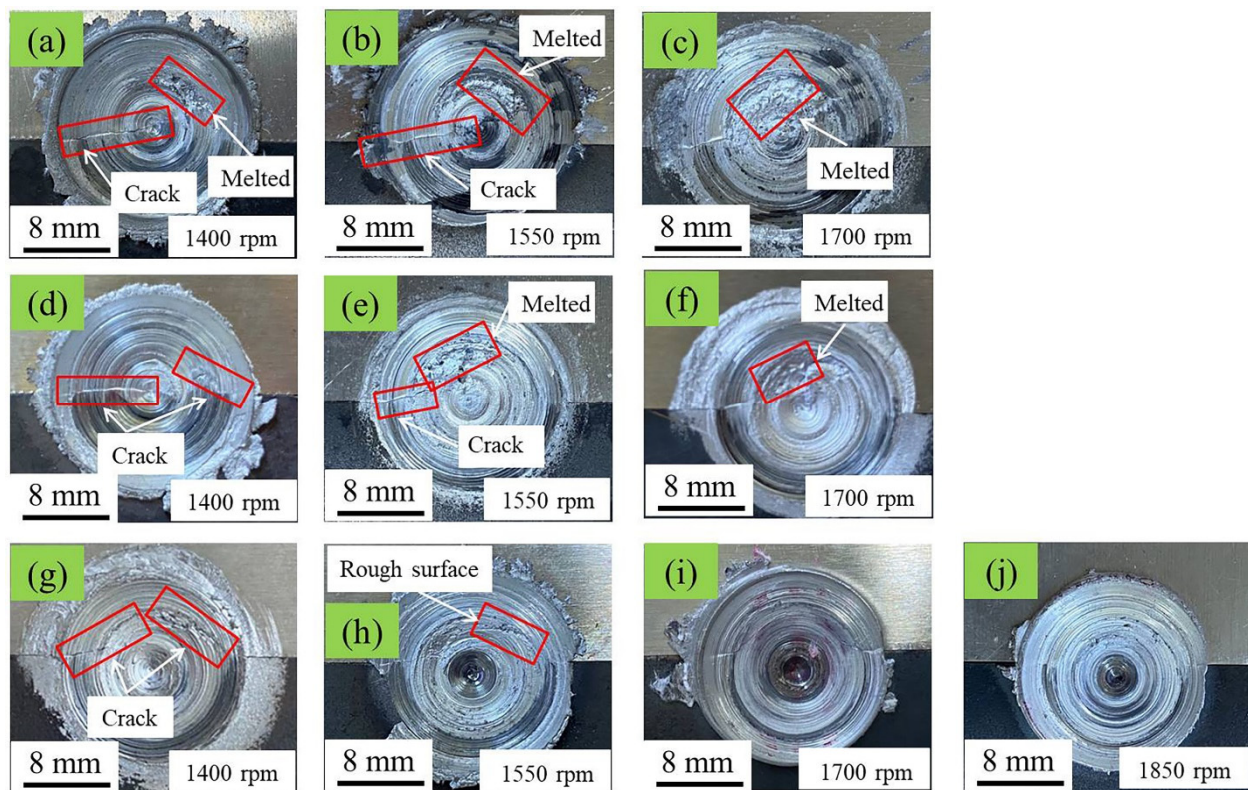


Figure 3. FSSW joints: (a–c) tool offset 1.5 mm toward the AA6061-T6 side, (d–f) no offset, and (g–j) tool offset 1.5 mm toward the S45C steel side.

Table 4. Observations of the weld surfaces under different parameter combinations.

No.	Tool Offset	Tool Rotational Speed (rpm)	Weld Quality
1	1.5 mm toward Al side	1400	Defective and melted
2		1550	Melted
3		1700	Melted
4	0	1400	Defective and melted
5		1550	Defective and melted
6		1700	Melted
7	+1.5 mm toward steel side	1400	Defective
8		1550	Good
9		1700	Good
10		1850	Good

Next, the tool position was shifted to the center of the weld between the S45C steel and the AA6061-T6 to diminish the excessive heating of the aluminum alloy. Unfortunately, the final results (Figure 3d–f) were similar to those obtained when the tool was offset to the AA6061-T6 side. Crack defects were still observed near the AA6061-T6/S45C joint interface. However, reducing the heat input to the aluminum alloy by shifting the tool position to the center of the weld certainly diminished the tendency of the AA6061-T6 to partially melt, as clearly shown in comparison to the results obtained with the relatively low tool rotational speed of 1400 rpm (Figure 3a,d). This suggests that properly distributing the heat input to the AA6061-T6 and the S45C steel by adjusting the tool offset can be helpful to prevent fusion defects in the joint.

Based on the trends observed in the experimental results shown in Figure 3a–f, the tool position was further offset (1.5 mm) to the S45C steel side. At the relatively low tool rotational speed of 1400 rpm (Figure 3g), obvious crack defects occurred at the interface

between the S45C steel and the AA6061-T6 due to the insufficient heat input. However, with this tool offset position, it was encouraging that the quality of the surface morphology was improved (i.e., the crack defects disappeared) by increasing the tool rotational speeds to 1550, 1700, and 1850 rpm without the occurrence of fusion defects, as presented in Figure 3h–j. This shows that for the given material combination of S45C steel and the AA6061-T6, offsetting the tool to the steel side was beneficial to produce a defect-free joint as it did not exhibit surface cracks and flaws related to solidification. By offsetting the tool to the steel side, more heat input could be applied to the steel without inducing fusion defects in the aluminum side.

The friction stir spot welded joints without cracks or fusion defects on the surface (Figure 3h–j) were further subjected to microstructural analysis. No significant difference in the OM results (Figure 4) was observed among the cross-sections of the joints made with three different FSSW parameter combinations except that the FSSW joint developed crack defects during welding at 1550 rpm (Figure 5a), but no significant defects were observed at the rotational speeds of 1700 and 1850 rpm, as shown in Figure 5b,c, respectively.

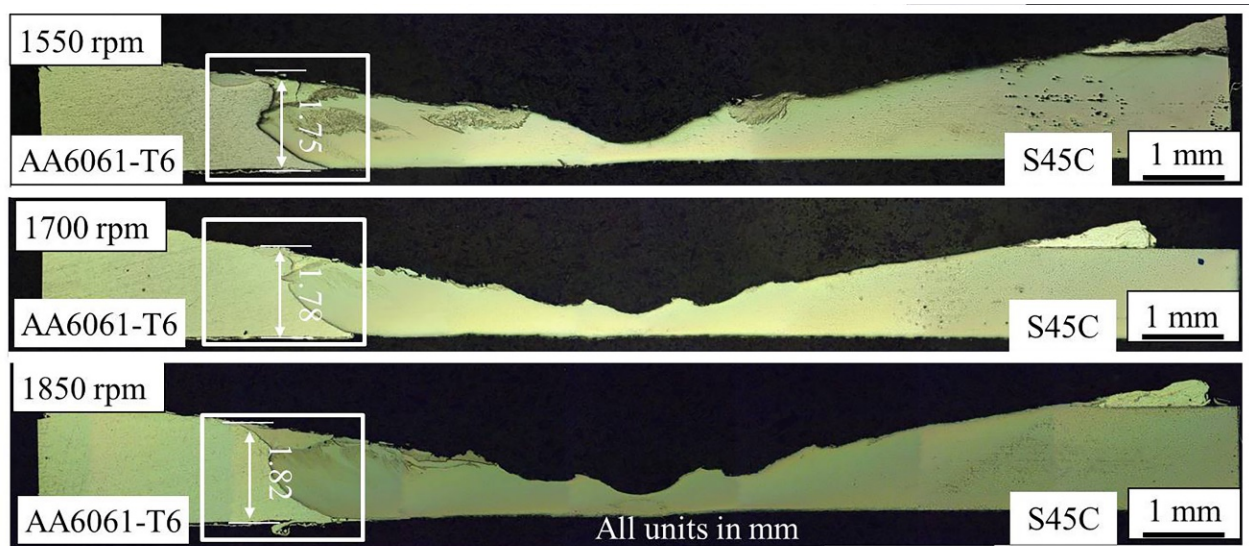


Figure 4. Optical macrographs of the weld cross-sections at three different tool rotational speeds (tool offset 1.5 mm toward the S45C steel side).

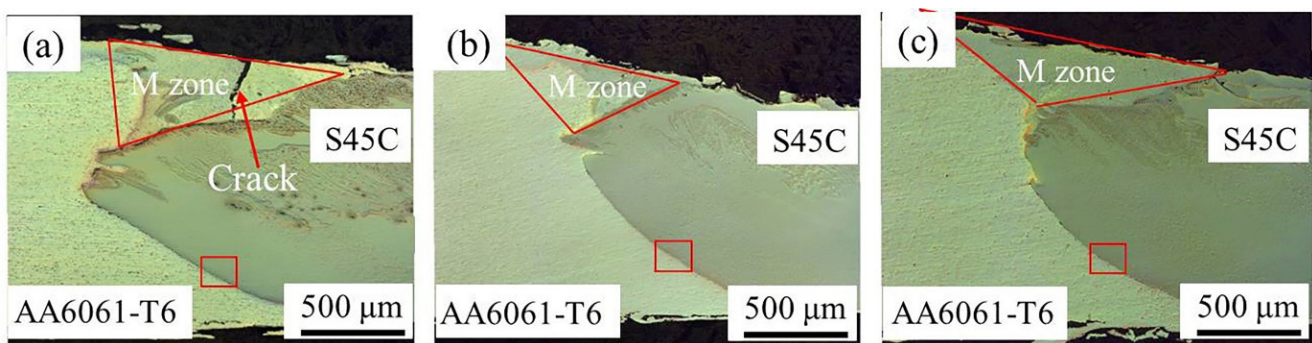


Figure 5. Magnified views of the regions marked by a white rectangle in Figure 4: (a) 1550 rpm, (b) 1700 rpm, and (c) 1850 rpm.

The regions marked with the red triangles (M zones = mixed zones) in Figure 5a–c exhibit a slightly different color compared with the S45C steel and AA6061-T6. The typical SEM image (Figure 6a) and the results of the EDS area scan (Figure 6b,c) suggest that the M zones were a mixture of aluminum alloy (green color) and steel particles (blue color).

This suggests that the plasticized aluminum alloy and numerous steel fragments peeled from the base metal were mechanically mixed into the M zone by the rotating tool. Further detailed characterization was carried out to observe the interdiffusion of Al and Fe between the AA6061-T6 and the S45C steel at the joint interface.

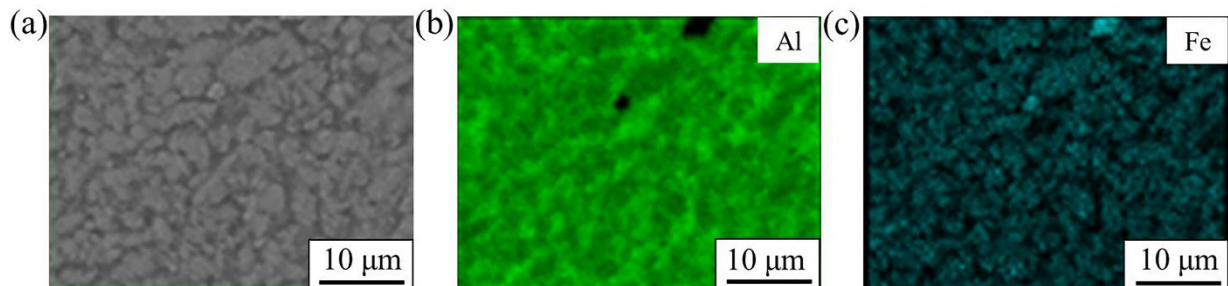


Figure 6. From Figure 5c: (a) SEM image of M zone, (b) Al distribution, and (c) Fe distribution.

As shown in Figures 4 and 5, an obvious boundary between the AA6061-T6 and the S45C steel was observed (except for the M zone at the top of the joint) for all three of the FSSW parameter combinations. The SEM results at the interface of the joints revealed a distinct layer with different colors between the S45C steel (bright region) and the AA6061-T6 (dark region) that was produced during welding at 1550 rpm (Figure 7a,b), 1700 rpm (Figure 8a,b), and 1850 rpm (Figure 9a,b).

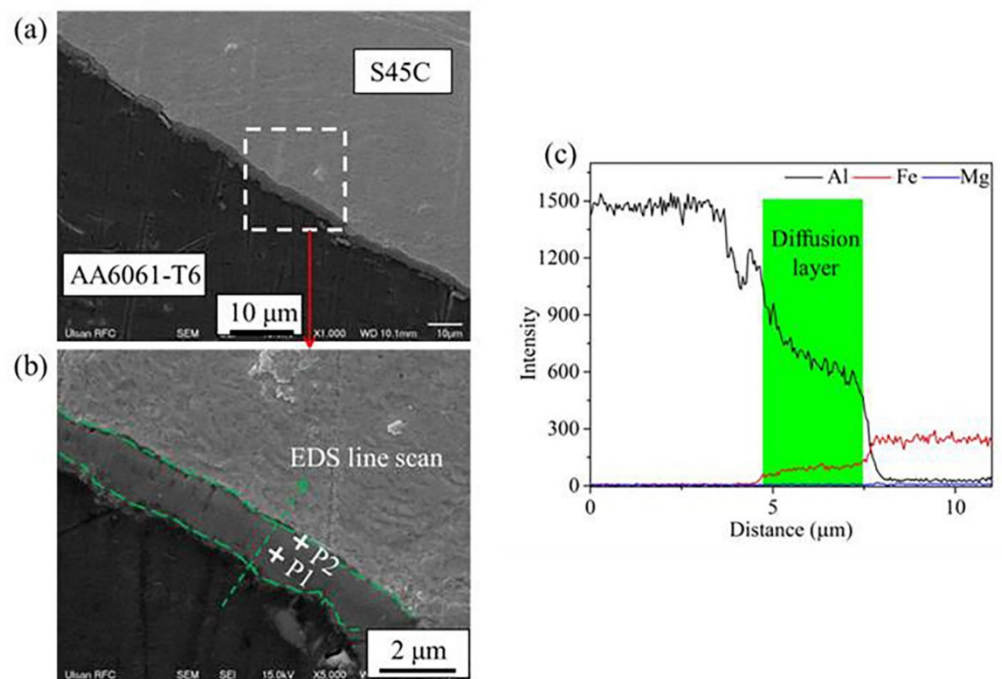


Figure 7. (a) SEM image of the region marked by a red rectangle in Figure 5a, (b) magnified SEM image of the joint interface (a white rectangle in (a)), and (c) elemental line scan across the joint interface.

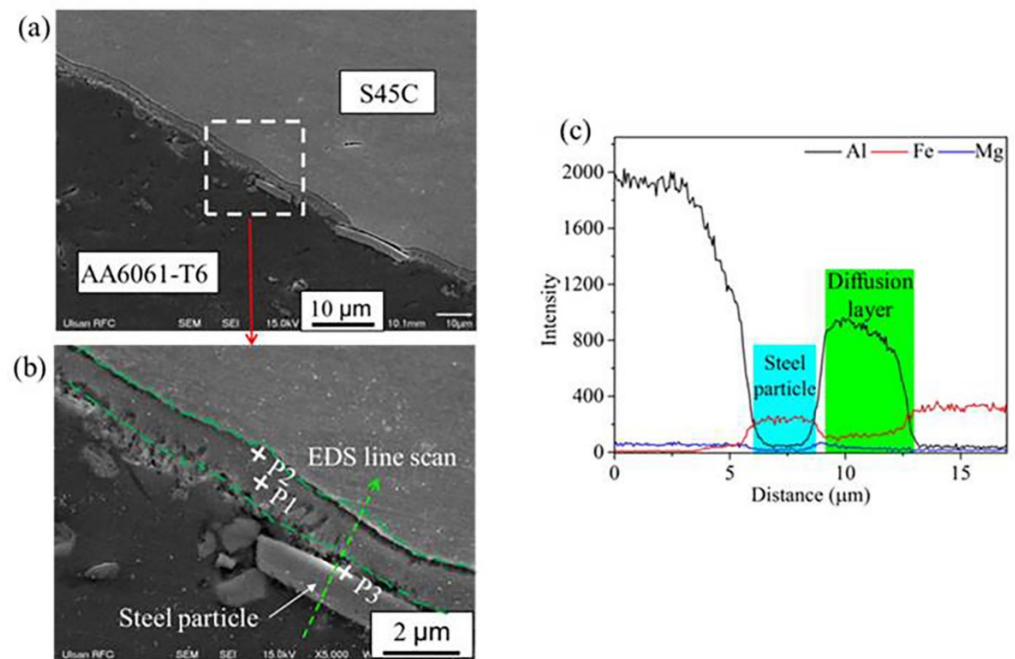


Figure 8. (a) SEM image of the region marked by a red rectangle in Figure 5b, (b) magnified SEM image of the joint interface (a white rectangle in (a)), and (c) elemental line scan across the joint interface.

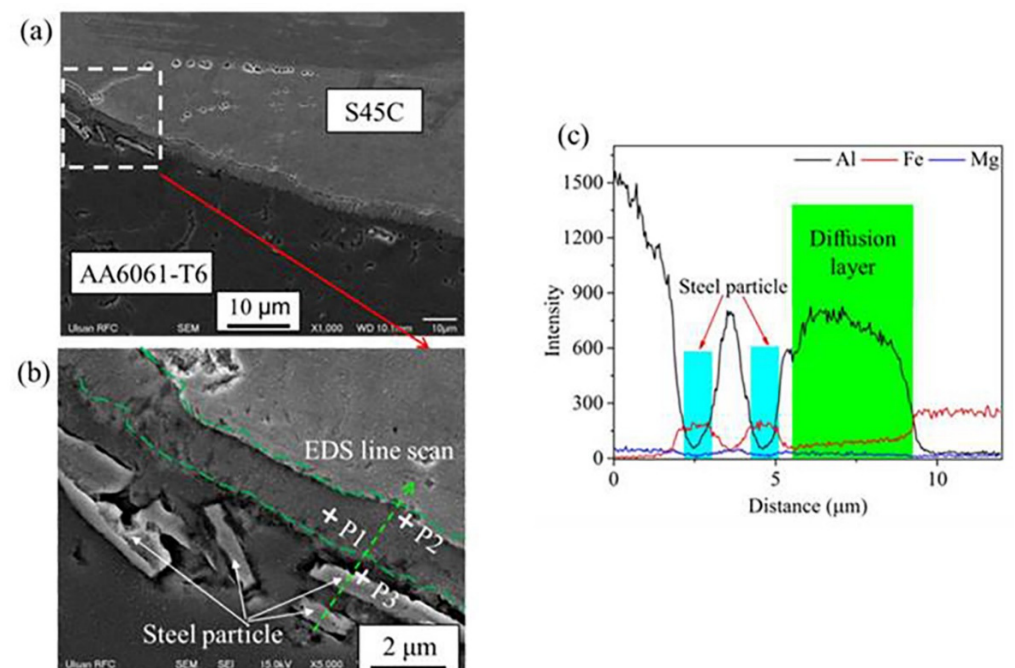


Figure 9. (a) SEM image of the region marked by a red rectangle in Figure 5c, (b) magnified SEM image of the joint interface (a white rectangle in (a)), and (c) elemental line scan across the joint interface.

The results of the EDS elemental line scan (Figures 7c, 8c and 9c) confirmed that the layers were composed of Al and Fe elements, which can be regarded as Al/Fe IMCs. Previous studies have suggested that atomic diffusion across the joint interface causes the formation of Al/Fe IMCs [16,24]. Further, in the present study, steel particles were observed on the Al side, as clearly shown in Figures 8b and 9b. Those steel particles could

have been the result of the detachment of steel fragments from the steel edges by high shear stress caused by the severe stirring motion of the tool at higher rotational speeds [31].

According to the Al–Fe phase diagram [32] and analysis of the EDS elemental compositions (in Table 5), the possible IMCs at the three different welding conditions can be deduced. As summarized in Table 5, the IMC layers in Figures 8b and 9b may have consisted of FeAl (Fe-rich IMCs) and FeAl₃ (Al-rich IMCs). In contrast, at the relatively lower rotational speed of 1550 rpm (Figure 7b), the IMC layer mainly included FeAl₃ and Fe₂Al₅ (Al-rich IMCs). With the increase in tool rotational speed, more Fe-rich IMCs (FeAl) were formed at the joint interface, which is not detrimental to the joint strength compared with Al-rich IMCs [27].

Table 5. Chemical compositions of IMC and possible phases in Figures 7–9.

Tool Rotational Speed (rpm)	Location	Composition (at.%)			Possible Phases	IMC Layer Thickness (μm) *
		Al	Fe	Al/Fe Ratio		
1550	P1	74.46	25.54	3.11	FeAl ₃	2.7 (± 0.8)
	P2	69.68	29.46	2.36	Fe ₂ Al ₅	
1700	P1	72.75	27.25	2.70	FeAl ₃	3.3 (± 1.0)
	P2	50.28	49.72	~1	FeAl	
	P3	48.43	51.57	~1	FeAl	
1850	P1	72.90	27.10	2.70	FeAl ₃	4.1 (± 1.1)
	P2	49.75	50.25	~1	FeAl	
	P3	46.25	53.75	~1	FeAl	

* Average value at three different locations.

The thickness of the IMC layer was approximated by the distribution of the major alloying elements across the interface through the EDS line scan, as shown in Figures 7c, 8c and 9c. When increasing the rotational speed from 1550 to 1850 rpm, a significant increase in the IMC layer thickness (from 2.7 to 4.6 μm) was observed. This indicates that a sufficient energy input or higher temperature can promote the diffusion of elements to the formation and growth of an Al/Fe IMC at the joint interface [24,33,34]. Still, in all of the FSSW conditions, the IMC layers formed at the joint interfaces were very thin.

Studies have shown that a thin IMC layer (less than 10 μm [10,12,35]) might not be detrimental to the mechanical properties of joints [11,24]. Here, the fractures in all of the friction stir spot welded joints occurred at the joining interface between the S45C steel and the AA6061-T6 after the tensile test (Figure 10b). As shown in the results of tensile tests (Figure 11), the maximum tensile strength of the friction stir spot welded joints (2830 ± 150 N) was obtained under the welding conditions of 1850 rpm. Note that the IMC layer of the friction stir spot welded joint created at the rotational speed of 1850 rpm was extremely thin (approximately 4.4 μm maximum thickness) compared with that of conventional fusion welding.

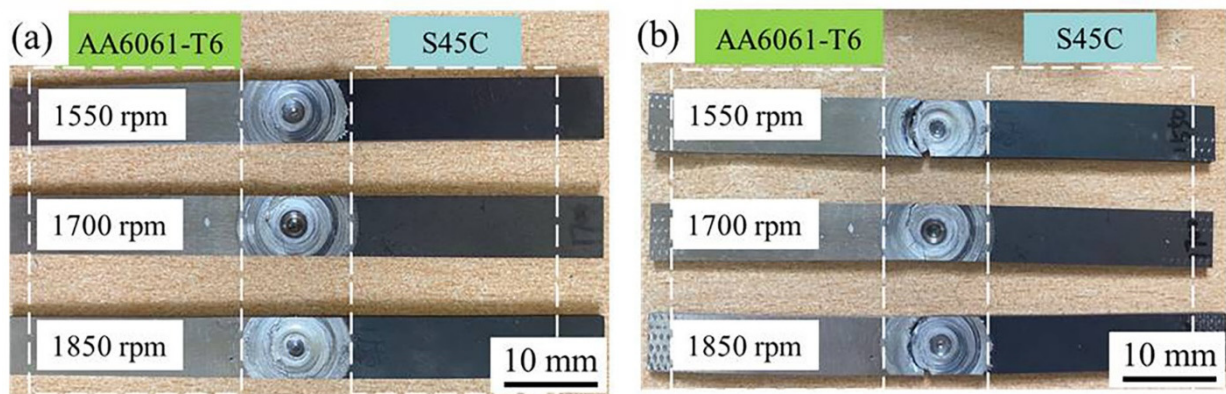


Figure 10. (a) Machined joint specimens and (b) tensile fractured specimens.

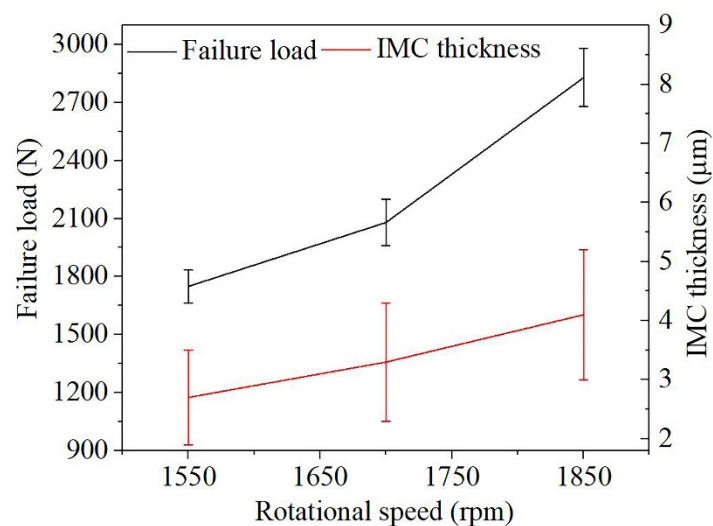


Figure 11. Thickness of IMC and joint failure load as functions of tool rotational speed.

The IMC layer and the failure load simultaneously increased with the increase in the tool rotational speed, as presented in Figure 11. The correlation of the tensile strength of the joint and the thickness of the IMC layer in Figure 11 confirms that in a certain range of thickness, a thicker IMC layer seems to improve the strength of the joint [24,36]. Bozzi et al. [26] agreed with this view that an IMC layer may be necessary to improve the friction stir spot welded weld strength of aluminum alloy and steel joints. Here, fracture during tensile tests occurred along the interface of the S45C steel and the AA6061-T6 and crossed over the M zone of the steel and the aluminum for all the FSSW joints (Figure 12a). Figure 12b shows that the thickness of the remaining IMC layer on the AA6061-T6 side was approximately 2 μm; in contrast, the fracture surface on the S45C steel side showed almost no remaining IMC, as shown in Figure 12c. To summarize, the tensile fracture failure of friction stir spot welded joints mainly occurred in the top Al/Fe mixing zone and in the interface between the S45C steel and the IMC layer.

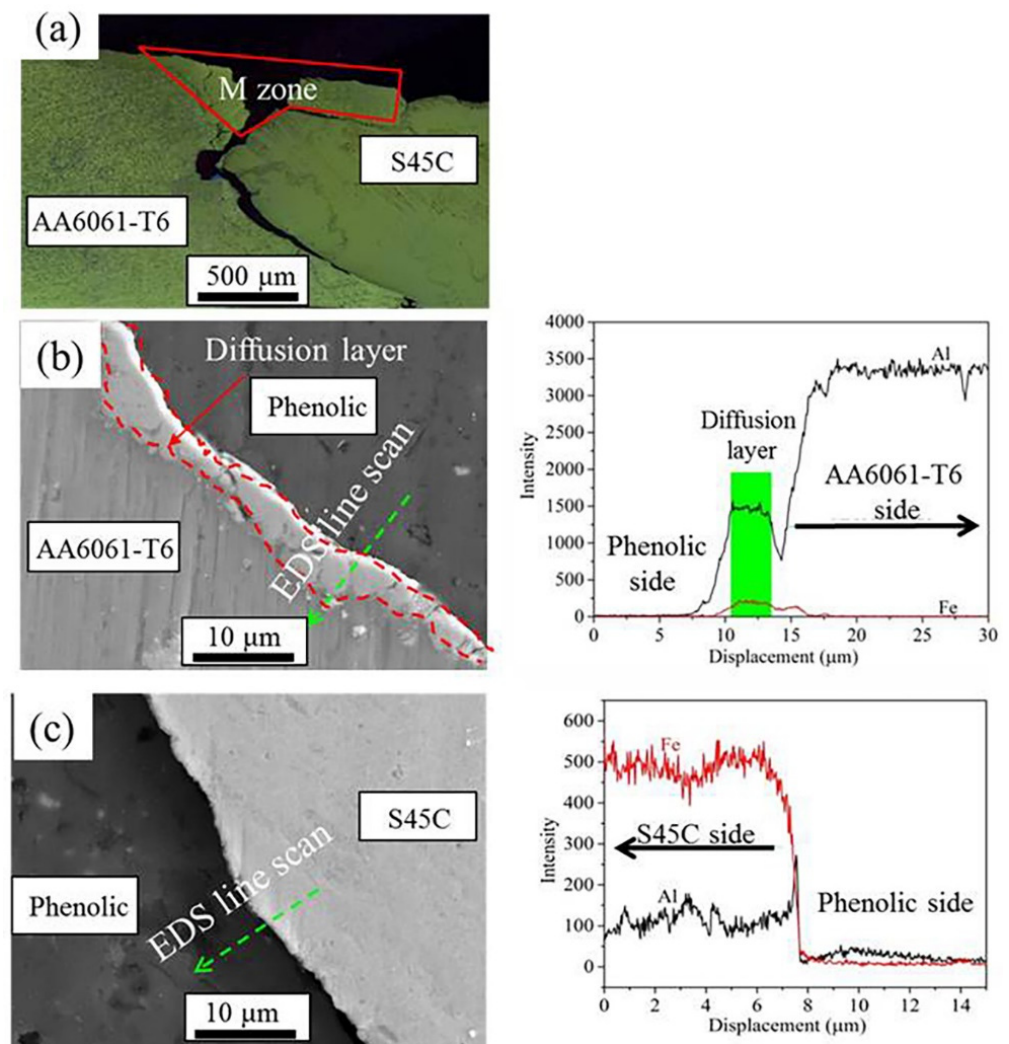


Figure 12. (a) A cross-sectional image of FSSW joints after tensile test (tool rotational speed of 1550 rpm); SEM images and elemental line scans on (b) the AA6061-T6 side and (c) the S45C side.

4. Conclusions

In the present work, FSSW of S45C steel and 6061-T6 aluminum alloy was conducted with different tool rotational speeds and tool positions. The experimental results showed that the friction stir spot welded butt joints of the dissimilar steel and the aluminum alloy were successfully fabricated by offsetting the tool by 1.5 mm toward the steel side. Microstructure analysis using SEM-EDS showed that an IMC layer was formed, and three possible IMCs (FeAl , FeAl_3 , and Fe_2Al_5) were identified at the joint interface. Increasing the tool rotational speed increased the thickness of the IMC layer. The results of point and line analysis suggested that a thicker IMC layer and Fe-rich IMCs seemed to be beneficial to improve the strength of the FSSW joints. The quasistatic tensile tests showed that fractures occurred along the joint interface and in the top Al/Fe mixing zone.

Author Contributions: Conceptualization, K.G. and S.-T.H.; methodology, K.G. and S.-T.H.; software, K.G.; validation, K.G., S.Z., S.-T.H., M.M., S.B. and H.S.; formal analysis, K.G. and S.-T.H.; investigation, K.G., S.Z. and S.-T.H.; resources, S.-T.H.; data curation, K.G., S.Z. and S.-T.H.; writing—original draft preparation, K.G.; writing—review and editing, S.-T.H.; supervision, S.-T.H.; project administration, S.-T.H.; funding acquisition, S.-T.H. All authors have read and agreed to the published version of the manuscript.

Funding: This research was funded by the 2021 research fund of the University of Ulsan.

Institutional Review Board Statement: Not applicable.

Informed Consent Statement: Not applicable.

Data Availability Statement: The raw/processed data required to reproduce these findings cannot be shared at this time as the data also form part of an ongoing study.

Acknowledgments: This work was supported by the 2021 research fund of the University of Ulsan.

Conflicts of Interest: The authors declare no conflict of interest.

References

1. Cole, G.S.; Sherman, A.M. Light weight materials for automotive applications. *Mater. Charact.* **1995**, *35*, 3–9. [[CrossRef](#)]
2. Schubert, E.; Klassen, M.; Zerner, I.; Walz, C.; Sepold, G. Light-weight structures produced by laser beam joining for future applications in automobile and aerospace industry. *J. Mater. Process. Technol.* **2001**, *115*, 2–8. [[CrossRef](#)]
3. Hussein, S.A.; Tahir, A.S.M.; Hadzley, A.B. Characteristics of Aluminum-to-Steel Joint Made by Friction Stir Welding: A review. *Mater. Today Commun.* **2015**, *5*, 32–49. [[CrossRef](#)]
4. Liu, X.; Lan, S.H.; Ni, J. Analysis of process parameters effects on friction stir welding of dissimilar aluminum alloy to advanced high strength steel. *Mater. Des.* **2014**, *59*, 50–62. [[CrossRef](#)]
5. Qiu, R.; Shi, H.; Zhang, K.; Tu, Y.; Iwamoto, C.; Satonaka, S. Interfacial characterization of joint between mild steel and aluminum alloy welded by resistance spot welding. *Mater. Charact.* **2010**, *61*, 684–688. [[CrossRef](#)]
6. Lin, S.B.; Song, J.L.; Ma, G.C.; Yang, C.L. Dissimilar metals TIG welding-brazing of aluminium alloy to galvanized steel. *Front. Mater. Sci. China* **2009**, *3*, 78–83. [[CrossRef](#)]
7. Chen, H.C.; Pinkerton, A.J.; Li, L.; Liu, Z.; Mistry, A.T. Gap-free fibre laser welding of Zn-coated steel on Al alloy for light-weight automotive applications. *Mater. Des.* **2011**, *32*, 495–504. [[CrossRef](#)]
8. Peyre, P.; Sierra, G.; Deschaux-Beaume, F.; Stuart, D.; Fras, G. Generation of aluminium-steel joints with laser-induced reactive wetting. *Mater. Sci. Eng. A* **2007**, *444*, 327–338. [[CrossRef](#)]
9. Mathieu, A.; Shabadi, R.; Deschamps, A.; Suery, M.; Mattei, S.; Grevey, D.; Cicala, E. Dissimilar material joining using laser (aluminum to steel using zinc-based filler wire). *Opt. Laser Technol.* **2007**, *39*, 652–661. [[CrossRef](#)]
10. Arghavani, M.R.; Movahedi, M.; Kokabi, A.H. Role of zinc layer in resistance spot welding of aluminium to steel. *Mater. Des.* **2016**, *102*, 106–114. [[CrossRef](#)]
11. Chen, N.; Wang, H.P.; Carlson, B.E.; Sigler, D.R.; Wang, M. Fracture mechanisms of Al/steel resistance spot welds in lap shear test. *J. Mater. Process Technol.* **2017**, *243*, 347–354. [[CrossRef](#)]
12. Miyamoto, K.; Nakagawa, S.; Sugi, C.; Sakurai, H.; Hirose, A. Dissimilar joining of aluminum alloy and steel by resistance spot welding. *SAE Int. J. Mater. Manuf.* **2009**, *2*, 58–67. [[CrossRef](#)]
13. Mustafa, A.; Bilge, D. An investigation of mechanical and metallurgical properties of explosive welded aluminum-dual phase steel. *Mater. Lett.* **2008**, *62*, 4158–4160.
14. Xue, J.Y.; Li, Y.X.; Chen, H.; Zhu, Z.T. Wettability, microstructure and properties of 6061 aluminum alloy/304 stainless steel butt joint achieved by laser-metal inert-gas hybrid welding-brazing. *Trans. Nonferrous Met. Soc. China* **2018**, *28*, 1938–1946. [[CrossRef](#)]
15. Meshram, S.D.; Mohandas, T.; Reddy, G.M. Friction welding of dissimilar pure metals. *J. Mater. Process. Technol.* **2007**, *184*, 330–337. [[CrossRef](#)]
16. Zhang, S.; Gao, K.; Hong, S.-T.; Ahn, H.; Choi, Y.; Lee, S.; Han, H.N. Electrically assisted solid state lap joining of dissimilar steel S45C and aluminum 6061-T6 alloy. *J. Mater. Res. Technol.* **2021**, *12*, 271–282. [[CrossRef](#)]
17. Findik, F. Recent developments in explosive welding. *Mater. Des.* **2011**, *32*, 1081–1193. [[CrossRef](#)]
18. Jiang, H.; Liao, Y.; Gao, S.; Li, G.; Cui, J. Comparative study on joining quality of electromagnetic driven self-piecing riveting, adhesive and hybrid joints for Al/steel structure. *Thin-Walled Struct.* **2021**, *164*, 107903. [[CrossRef](#)]
19. Thomas, W.M.; Nicholas, E.D.; Needham, J.C.; Murch, M.G.; Temple-Smith, P.; Dawes, C.J. Friction Stir Butt Welding. International Patent Application No. PCT/GB92/02203 and GB Patent Application No. 9125978.8, 6 December 1991.
20. Rai, R.; De, A.; Bhadeshia, H.K.D.H.; DebRoy, T. Review: Friction stir welding tools. *Sci. Technol. Weld Join.* **2011**, *16*, 325–342. [[CrossRef](#)]
21. Wang, L.; Huang, Y.X. Friction stir welding of dissimilar aluminum alloys and steels: A review. *Int. J. Adv. Manuf. Technol.* **2018**, *99*, 1781–1811.
22. Watanabe, T.; Takayama, H.; Yanagisawa, A. Joining of aluminum alloy to steel by friction stir welding. *J. Mater. Process. Technol.* **2006**, *178*, 342–349. [[CrossRef](#)]
23. Kimapong, K.; Watanabe, T. Lap Joint of A5083 aluminum alloy and SS400 steel by friction stir welding. *Mater. Trans.* **2005**, *46*, 835–841. [[CrossRef](#)]
24. Fereiduni, E.; Movahedi, M.; Kokabi, A.H. Aluminum/steel joints made by an alternative friction stir spot welding process. *J. Mater. Process. Technol.* **2015**, *224*, 1–10. [[CrossRef](#)]
25. Coelho, R.S.; Kostka, A.; Dos Santos, J.F.; Kaysser-Pyzalla, A. Friction-stir dissimilar welding of aluminum alloy to high strength steels: Mechanical properties and their relation to microstructure. *Mater. Sci. Eng. A* **2012**, *556*, 175–183. [[CrossRef](#)]

26. Bozzi, S.; Helbert-Etter, A.L.; Baudin, T.; Criqui, B.; Kerbiguet, J.G. Intermetallic compounds in Al 6016/IF-steel friction stir spot welds. *Mater. Sci. Eng. A* **2010**, *527*, 4505–4509. [[CrossRef](#)]
27. Pourali, M.; Abdollah-zadeh, A.; Saeid, T.; Kargar, F. Influence of welding parameters on intermetallic compounds formation in dissimilar steel/aluminum friction stir welds. *J. Alloys Compd.* **2017**, *715*, 1–8. [[CrossRef](#)]
28. Kaushik, P.; Dwivedi, D.K. Effect of tool geometry in dissimilar Al-steel friction stir welding. *J. Manuf. Process.* **2021**, *68*, 198–208. [[CrossRef](#)]
29. Jeon, C.S.; Hong, S.-T.; Kwon, Y.J.; Cho, H.H.; Han, H.N. Material properties of friction stir spot welded joints of dissimilar aluminum alloys. *Trans. Nonferrous Met. Soc. China.* **2012**, *22*, s605–s613. [[CrossRef](#)]
30. Yuan, W.; Mishra, R.S.; Webb, S.; Chen, Y.L.; Carlson, B.; Herling, D.R.; Grant, G.J. Effect of tool design and process parameters on properties of Al alloy 6016 friction stir spot welds. *J. Mater. Process. Technol.* **2011**, *211*, 972–977. [[CrossRef](#)]
31. Zandsalimi, S.; Heidarzadeh, A.; Saeid, T. Dissimilar friction-stir welding of 430 stainless steel and 6061 aluminum alloy: Microstructure and mechanical properties of the joints. *Proc. Inst. Mech. Eng. Part L J. Mater. Des. Appl.* **2019**, *233*, 1791–1801. [[CrossRef](#)]
32. Sina, H.; Corneliusson, J.; Turba, K.; Iyengar, S. A study on the formation of iron aluminide (FeAl) from elemental powders. *J. Alloys Compds.* **2015**, *636*, 261–269. [[CrossRef](#)]
33. Sundman, B.; Ohnuma, I.; Dupin, N.; Kattner, U.R.; Fries, S.G. An assessment of the entire Al-Fe system including D03 ordering. *Acta Mater.* **2009**, *57*, 2896–2908. [[CrossRef](#)]
34. Chmielewski, T.; Marcin Chmielewski, O.; Piątkowska, A.; Grabias, A.; Beata Skowrońska, O.; Siwek, P. Phase Structure Evolution of the Fe-Al Arc-Sprayed Coating Stimulated by Annealing. *Materials* **2021**, *14*, 3210. [[CrossRef](#)] [[PubMed](#)]
35. Tanaka, T.; Nezu, M.; Uchida, S.; Hirata, T. Mechanism of intermetallic compound formation during the dissimilar friction stir welding of aluminum and steel. *J. Mater. Sci.* **2020**, *55*, 3064–3072. [[CrossRef](#)]
36. Tanaka, T.; Hirata, T.; Shinomiya, N.; Shirakawa, N. Analysis of material flow in the sheet forming of friction-stir welds on alloys of mild steel and aluminum. *J. Mater. Process. Technol.* **2015**, *226*, 115–124. [[CrossRef](#)]